Gyrokinetic modeling of ion transport anomalies on electron-heated ASDEX Upgrade L-modes

M. M. Skyllas[1], B. Brandström[1], P. Strand[1], D. Yadykin[1], R. Fischer[2] and the ASDEX Upgrade team[2,a]
[1]Department of Space, Earth and Environment, Chalmers University of Technology
[2]Max-Planck-Institüt für Plasmaphysik, Boltzmannstraße 2, Garching D-85748, Germany
[a] see author list of T. Püttelich *et al.* Nucl. Fusion **66** 116002 (2026)

The TGLF-SAT2 model systematically over-predicts ion heat flux in electron-heated ASDEX Upgrade L-mode plasmas [1]. This study investigates this discrepancy using non-linear GENE simulations of discharge #35475 across NBI, mixed, and ECRH-dominated heating phases. By comparing gyrokinetic outputs against integrated modeling, we aim to recover the lower experimental ion heat transport observed during ECRH. We specifically analyze the evolution of τ and its impact on the turbulence spectrum [4, 8, 9] to isolate physics missing from reduced models. Ultimately, these insights will inform and improve future saturation rules.

1 Introduction

The development of accurate reduced-order transport models is critical for future fusion reactors. While recent updates like TGLF-SAT2 have successfully resolved the "L-mode shortfall" in standard regimes [12], significant gaps remain. Specifically, in electron-heated ASDEX Upgrade (AUG) plasmas, TGLF-SAT2 systematically over-predicts the ion heat flux, leading to an under-prediction of ion stored energy [1]. This discrepancy highlights a failure in current saturation rules when strong ion heating is absent. Resolving this transport anomaly requires a fundamental approach. This study utilizes the nonlinear, flux-tube gyrokinetic code GENE [7] to investigate the turbulence mechanisms at play. By testing whether high-fidelity gyrokinetic simulations can recover the experimentally observed lower ion heat transport, we will establish the physics basis necessary to correct and improve future integrated modeling efforts.

1.1 The discharge

The ASDEX Upgrade discharge #35475 was selected as the primary subject of this investigation, to systematically isolate the onset of the transport anomaly. It is a deuterium discharge with carbon impurities that provides an ideal testing ground due to its extended flat-top phase, which is divided into three distinct and stable heating regimes.

- Phase I (NBI-dominated): The baseline phase driven by Neutral Beam Injection, representing a regime wherer reduced transport models like TGLF-SAT2 typically exhibit good agreement with experimental power balance.

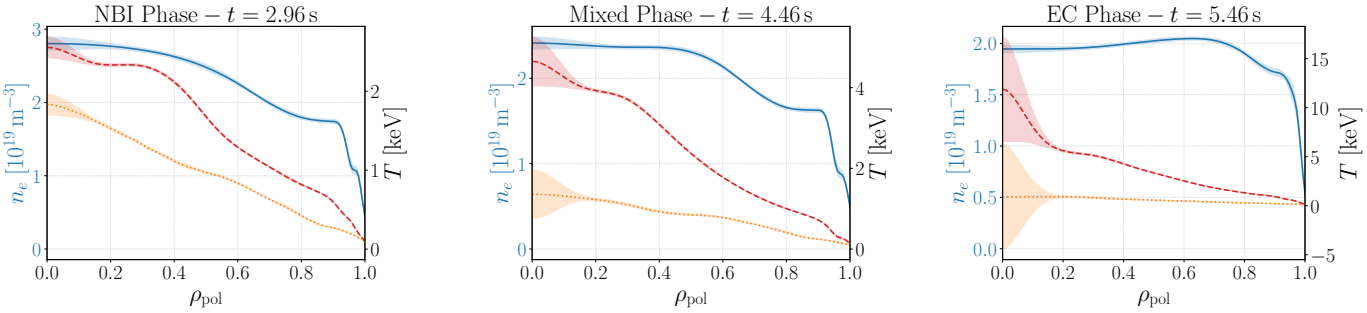

Figure 1: Kinetic profiles of the electrons and ions at $t = 2.96$ s (NBI, left), $t = 4.46$ s (Mixed, middle), $t = 5.46$ s (EC, right). The vertical green line denotes the radial coordinate simulated ($\rho = 0.3/\rho_{\mathrm{pol}} = 0.41$).

- Phase II (Mixed heating): A transitional phase featuring a balanced heating mix of 50% NBI and 50% Electron Cyclotron Resonance Heating (ECRH).
- Phase III (ECRH-dominated): This the phase of interest for this study where the heating is shifted predominantly to the electrons, and where the TGLF-SAT2 ion heat flux over-prediction explicitly manifests.

1.2 The evolution of the τ parameter

The transition through the three heating phases dynamically changes the ratio of electron-to-ion heating and thereby, significantly alters the temperature ratio $T_\mathrm{i}/T_\mathrm{e}$, or its gyrokinetic equivalent which enters the equations as $\tau = T_\mathrm{e}/(Z_\mathrm{eff}T_i)$, where $Z_\mathrm{eff} = n_\mathrm{e}^{-1}\sum_i n_i q_i^2$ is the effective ion charge. Such drastic changes in the temperature ratio can heavily affect the turbulence spectrum [4, 8, 9]. To ensure the simulations remain consistent with the state of the plasma at every phase of the discharge, the experimental data for the plasma parameters and the numerical equilibrium of the geometry are provided as input through an interface that converts IMAS data to Gene input. That allows for the continuous tracking of τ across the changes in the plasma, as well as the modes that exist during each phase.

2 Experimental data and simulation setup

To investigate the TGLF-SAT2 shortfall, macroscopic profile data from ASDEX Upgrade #35475 are translated into a local gyrokinetic framework. Constrained MHD magnetic equilibria are reconstructed for each of the three heating phases. Thermodynamic driving forces, including normalized radial gradients and the temperature ratio (τ), are derived from IMAS database profiles, with uncertainties quantified via an MCMC method [5].

Turbulent transport is modeled using the flux-tube limit of Gene [7] with kinetic electrons, deuterium, and carbon. Linear simulations at the core radius ($\rho = 0.3$) for $0.1 < k_y\rho_\mathrm{s} < 3.2$ characterize microinstabilities across all heating phases. Subsequently, 5D convergence-tested nonlinear simulations are performed. Time-averaged saturated fluxes are extracted for comparison against integrated modeling workflows, and spectral diagnostics are utilized to assess nonlinear saturation mechanisms such as zonal flows.

3 Results

In this section we aim to characterize the dominant instability present during each heating phase of the discharge at the three aforementioned radial points, and evaluate their sensitivity with respect to the spatially and temporally changing τ. A linear stability analysis is always of paramount importance, serving as the precursor to the state of the turbulence in the nonlinear state. The existence of multiple unstable modes, or lack thereof can significantly affect the saturation level of the turbulent fluxes of the electron or the ion channel. Furthermore, the evolution of the turbulence when the nonlinearity takes over can provide insight into what nonlinear phenomena govern the physics, which will be informative of where the integrated modeling techniques lack in their attempt to capture the physics that determine the saturation level of the fluxes.

All the linear initial value simulations use the experimental data to calculate the values of the plasma parameters. The box length in the radial and binormal directions is calculated automatically through Gene to maximize the number of connections of the modes, which pertains to the parallel boundary condition implemented in the code. The coordinates $(k_x, k_y, z, v_\parallel, \mu)$ are resolved with a minimum grid of $32 \times 1 \times 32 \times 32 \times 8$ points, with a few exceptions where it was necessary to double the number of points in the parallel direction coordinate or the number of k_x modes.

t	ρ	T_e	T_i	ω_n	ω_{Te}	ω_{Ti}	q_0	$\hat{s}$	β
2.96	0.3	1.0	0.761	0.723	2.561	1.778	1.423	0.252	0.003
	0.6	1.0	0.973	0.908	1.775	2.160	2.065	1.05	0.001
	0.9	1.0	0.912	4.925	7.656	3.450	4.553	3.137	0.0001

Table 1: Plasma parameters during each heating phase across the radial points simulated (in Gene normalized units).

The main plasma parameters of the NBI phase are summarized in Table 1. The gradients attain moderate values before the edge, where those values see at least a twofold increase. The linear initial value Gene output is shown in Figure 2, where each panel corresponds to simulations conducted at the plasma core radial location $\rho = 0.3$,

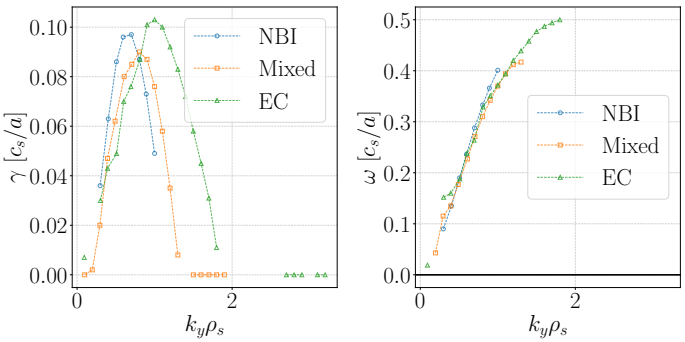

Figure 2: Growth rate (left) and frequency (right) spectra for the three heating phases at $\rho = 0.3$.

during the NBI, mixed and EC heating phase, by mapping them to the corresponding value of the τ parameter and depicts the growth rate and the frequency of the dominant instability within a binormal wavenumber range of $0.1 < k_y\rho_s < 2.0$.

The growth rate spectra consist of modes being destabilized at different spatial scales. Modes unstable at long wavelengths Figure 2, i.e., the ion-scale ($0.1 \leq k_y\rho_s \leq 1.2$) propagating at the ion diamagnetic drift direction, and modes at moderate-to-short wavelengths ($1.5 \leq k_y\rho_s \leq 3.2$) propagating at the electron diamagnetic drift direction (subdominant modes resulting from eigenvalue simulations - not shown).

The ion-direction propagating mode exhibits ITG characteristics, a claim which is supported by the influence β exerts on the growth rates, as long as $\beta < \beta_{\text{crit}}^{\text{KBM}}$, visualized in Figure 3. ITG can be linearly stabilized by higher β due to magnetic field line bending induced by electromagnetic perturbations [10, 2, 11], which is reflected on the figure in which the ion-scale growth rates experience a slight increase when β is decreased from the nominal value to 75% and 50% thereof. The opposite is recorded when the parameter is enhanced to 125% of its original value.

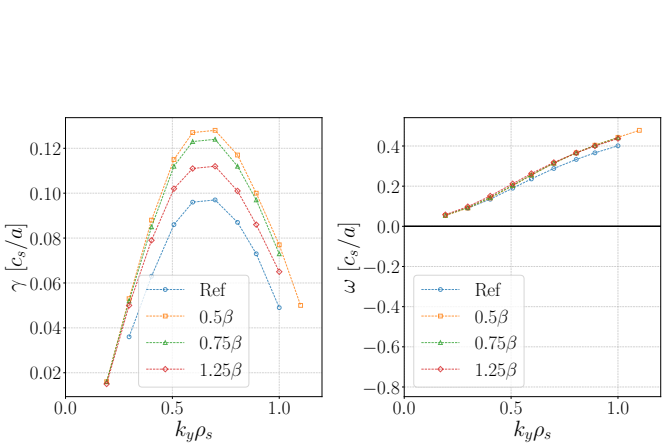

(a) Growth rate and frequency spectra of the ion-diamagnetic-direction propagating mode for varying β values.

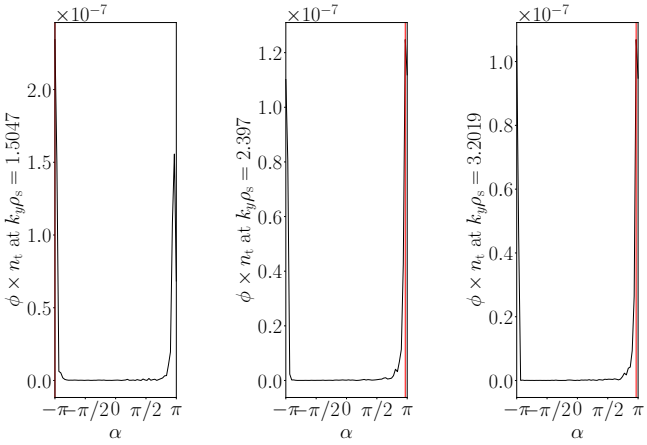

(b) Cross-phase between the electrostatic potential and trapped electron density perturbations at $k_y = 1.5, 2.4$, and 3.2.

Figure 3: Growth rate spectra response to a β variation in the ion-scale to assess the effect of electromagnetic perturbations (left). Cross-phases of the electrostatic potential and trapped-electron density perturbations to probe whether particle flux is expected to be generated by the instability (right).

The identification of the unstable modes in the electron scale requires a greater level of detail. ∇T-TEM and ETG are very challenging to distinguish. One of the fundamental differences between the two instabilities is the particle flux driven by the TEM [6]. While absolute particle flux can be measured in nonlinear simulations, the cross-phase between the electrostatic potential and the trapped-particle density acts as a reliable linear proxy, shown in Figure 3b. The three panels correspond to $k_y\rho_s = 1.5,\ 2.4$, and 3.2, respectively. It becomes abundantly clear that for the dominant mode detected in Figure 2, the criterion for particle flux production is not met at any of the wavenumbers under examination. Therefore, we consider the mode in question to be identified as an ETG.

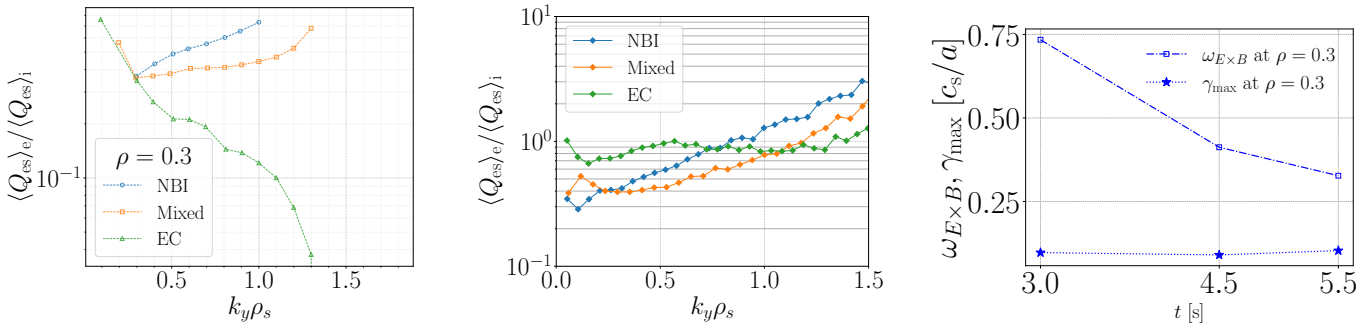

Figure 4: Electron-to-ion heat flux ratio spectrum calculated quasilinearly (left) and nonlinearly (middle). Nonlinear $\mathbf{E}\times\mathbf{B}$ shearing rates and the maximum growth rate from each heating phase (right).

The anomaly observed during the EC-heated phase aligns with quasilinear electron-to-ion heat flux ratios dropping below 0.1, contrasting with the near-unity ratios of the NBI and mixed phases (Figure 4, left panel). However, nonlinear spectra diverge sharply from these quasilinear estimates, exhibiting a gradual increase at higher wavenumbers that indicates dominant electron heat transport, with the EC-phase nonlinear flux remaining near unity (middle panel). This discrepancy likely stems from zonal flows dominating turbulence suppression in the saturated state [3]. Even though the nonlinear $\mathbf{E}\times\mathbf{B}$ shearing rate is weakest during the EC phase, it remains three to seven times larger than the maximum linear growth rate, suggesting that resolving this anomaly requires adjusting the saturation rules in integrated modeling codes to accurately capture high-τ saturated states.

4 Conclusions

Gyrokinetic modeling of ASDEX Upgrade discharge #35475 using the GENE code investigates the overprediction of ion heat transport by TGLF-SAT2 in electron-heated regimes. While linear simulations exhibit an ITG-dominated state that aligns with the exaggerated ion heat transport, nonlinear analyses demonstrate that ITG/TEM mixing and zonal flow generation significantly moderate overall heat fluxes. Incorporating these nonlinear effects—which are notably absent in quasilinear models—offers a potential resolution to the originally reported transport anomalies.

Future research will expand these gyrokinetic simulations across broader radial and temporal domains to establish consistent trends. Furthermore, planned power balance studies and comparisons of growth rates and flux spectra against ETS/TGLF will evaluate whether GENE-predicted heat fluxes match experimental power inputs and determine how experimental profile evolution impacts these predictions.

5 Acknowledgments

This work was supported by the Swedish Energy Agency [grant number P2023-01345]. This work has been carried out within the framework of the EUROfusion Consortium, funded by the European Union via the Euratom Research and Training Programme (Grant Agreement No 101052200 — EUROfusion). Views and opinions expressed are however those of the author(s) only and do not necessarily reflect those of the European Union or the European Commission. Neither the European Union nor the European Commission can be held responsible for them. The author thankfully acknowledges the computer resources at MareNostrum and the technical support provided by Barcelona Supercomputing Center (RES-AECT-2014-2-0085). The computations/data handling were enabled by resources provided by the National Academic Infrastructure for Supercomputing in Sweden (NAISS), partially funded the Swedish Research Council through grant agreement no. 2022-06725.

References

[1] C. Angioni et al. en. *Nuclear Fusion* 62.6 (2022).
[2] J. Candy. en. *Physics of Plasmas* 12.7 (2005).
[3] J. Chowdhury et al. en. *Physics of Plasmas* 19.10 (2012).
[4] H Doerk et al. *Plasma Physics and Controlled Fusion* 58.11 (2016).
[5] R. Fischer et al. en. *Fusion Science and Technology* 76.8 (2020).
[6] X. Garbet et al. *Nuclear Fusion* 50 (2010).
[7] F. Jenko et al. *Physics of Plasmas* 7.5 (2000).
[8] Z Lin et al. *Plasma Physics and Controlled Fusion* 49.12B (2007).
[9] A. G. Peeters et al. en. *Physics of Plasmas* 12.7 (2005).
[10] M. J. Pueschel et al. *Physics of Plasmas* 15.10 (2008).
[11] M. J. Pueschel et al. en. *Physics of Plasmas* 17.6 (2010).
[12] G.M. Staebler et al. en. *Nuclear Fusion* 64.8 (2024).